Electronic Supplementary Material (ESI) for RSC Advances.

Supporting Information

Extended visible photosensitivity of carboxyethyltin functionalized polyoxometalates with common organic dyes enabling enhanced photoelectric performance

1. **Crystal structure figures**
2. **Selected bond lengths and angles of SnR-Cu-P_2W_{15} and SnR-Zn-P_2W_{15}**
3. **Chemical and Physical characterizations**

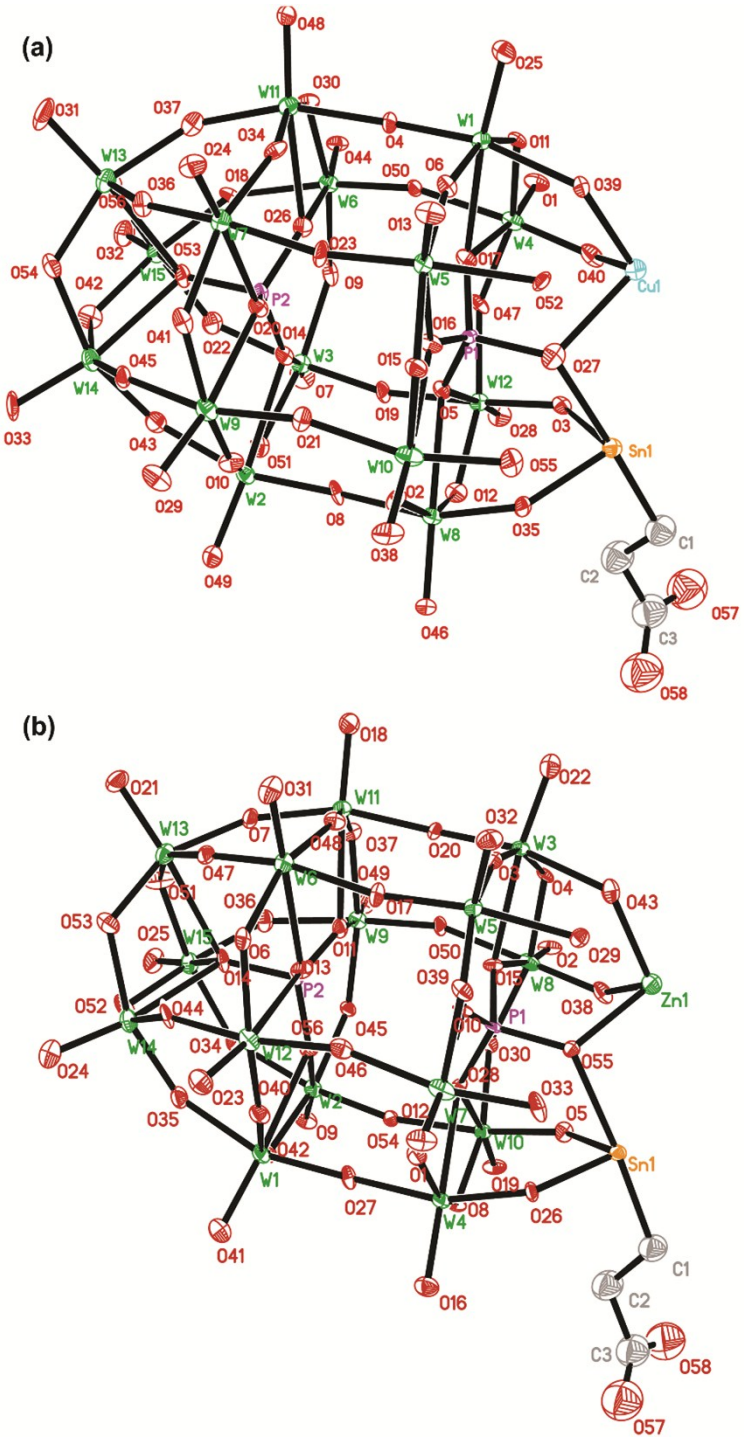

Fig. S1. ORTEP drawing of polyoxoanions of SnR-Cu-P_2W_{15} (a) and SnR-Zn-P_2W_{15} (b) with thermal ellipsoids at 30 % probability (H atoms, $[C(NH_2)_3]^+$ cations and free water molecules have been omitted for clarity)

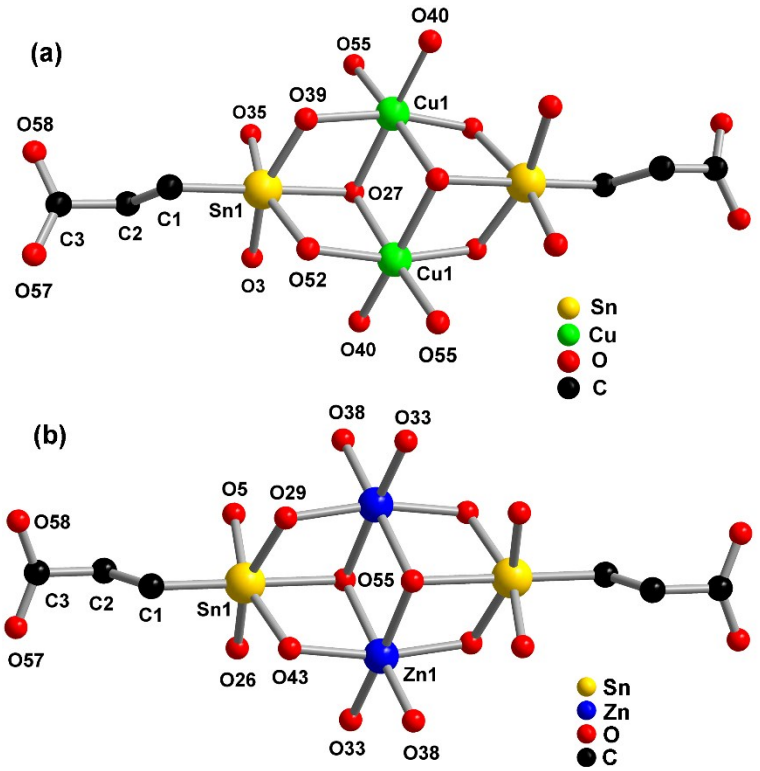

Fig. S2. Ball-and-stick representation of the central $\{(Sn(CH_2)_2COO)_2Cu_2O_{14}\}$ and $\{(Sn(CH_2)_2COO)_2Zn_2O_{14}\}$ fragments of SnR-Cu-P_2W_{15}(a) and SnR-Zn-P_2W_{15} (b)

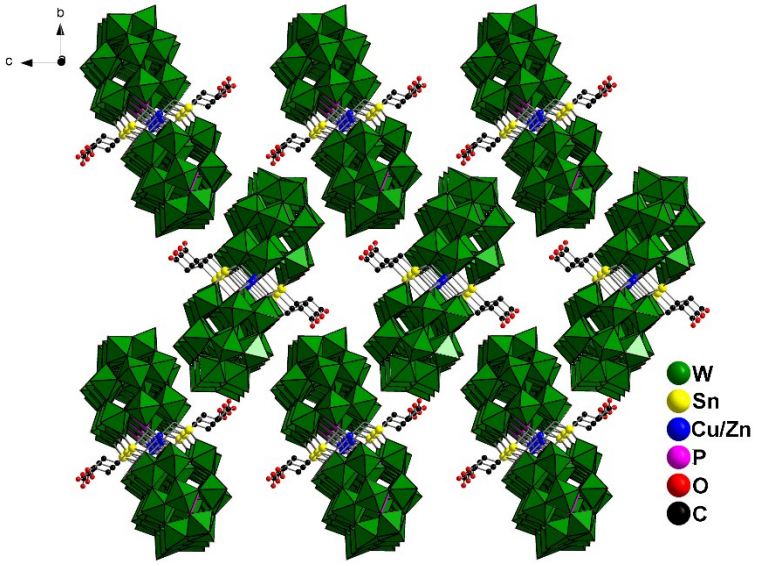

Fig. S3. The packing arrangement of the polyoxoanions in SnR-Cu-P_2W_{15} or SnR-Zn-P_2W_{15} (all H atoms, the isolated $[C(NH_2)_3]^+$ cations and water molecules existed in the interspaces are omitted for clarity)

2. Selected bond lengths and angles of SnR-Cu-P_2W_{15} and SnR-Zn-P_2W_{15}

Table S1 Selected bond lengths (Å) and angles (°) for SnR-Cu-P_2W_{15}

Bond	**Length (Å)**	**Bond**	**Length (Å)**	**Bond**	**Length (Å)**
W1–O25	1.701(14)	W7–O34	1.903(13)	W13–O36	1.957(12)
W1–O4	1.842(12)	W7–O41	1.924(13)	W13–O53	2.396(13)
W1–O11	1.878(12)	W7–O23	1.949(12)	W14–O33	1.729(13)
W1–O6	1.914(12)	W7–O20	2.358(13)	W14–O45	1.841(13)
W1–O39	2.080(12)	W8–O46	1.704(13)	W14–O43	1.849(14)
W1–O17	2.353(13)	W8–O35	1.800(12)	W14–O42	1.943(13)
W2–O49	1.719(14)	W8–O2	1.916(13)	W14–O54	1.978(14)
W2–O8	1.815(13)	W8–O12	1.925(13)	W14–O53	2.360(12)
W2–O51	1.902(14)	W8–O8	1.996(13)	W15–O32	1.703(15)
W2–O10	1.916(14)	W8–O5	2.383(12)	W15–O22	1.857(14)
W2–O43	2.011(13)	W9–O29	1.704(13)	W15–O18	1.860(12)
W2–O14	2.391(12)	W9–O21	1.837(13)	W15–O42	1.954(14)
W3–O7	1.724(14)	W9–O10	1.858(14)	W15–O56	1.965(16)
W3–O19	1.821(13)	W9–O41	1.946(14)	W15–O53	2.370(12)
W3–O51	1.916(13)	W9–O45	2.020(13)	Sn1–O3	2.056(13)
W3–O9	1.917(13)	W9–O20	2.326(12)	Sn1–O39#1	2.060(13)
W3–O22	1.991(14)	W10–O38	1.713(13)	Sn1–O35	2.064(13)
W3–O14	2.357(13)	W10–O55	1.803(14)	Sn1–O52#1	2.065(13)
W4–O1	1.705(13)	W10–O2	1.868(14)	Sn1–C1	2.12(3)
W4–O40	1.797(15)	W10–O15	1.962(13)	Sn1–O27	2.290(14)
W4–O47	1.881(12)	W10–O21	2.017(12)	Cu1–O40	2.005(15)
W4–O11	1.963(12)	W10–O16	2.355(12)	Cu1–O55#1	2.018(14)
W4–O50	2.066(12)	W11–O48	1.683(14)	Cu1–O52#1	2.085(12)
W4–O17	2.360(12)	W11–O37	1.871(14)	Cu1–O39	2.117(13)
W5–O13	1.704(13)	W11–O30	1.888(13)	Cu1–O27#1	2.237(14)
W5–O23	1.835(12)	W11–O34	1.891(12)	Cu1–O27	2.241(15)
W5–O15	1.854(12)	W11–O4	1.942(12)	P1–O16	1.515(13)
W5–O6	1.894(12)	W11–O26	2.392(14)	P1–O5	1.521(13)
W5–O52	2.076(12)	W12–O28	1.684(13)	P1–O17	1.543(13)
W5–O16	2.361(12)	W12–O3	1.819(13)	P1–O27	1.619(15)
W6–O44	1.708(13)	W12–O12	1.912(13)	P2–O14	1.521(14)
W6–O50	1.811(12)	W12–O47	1.929(12)	P2–O26	1.522(13)
W6–O9	1.867(14)	W12–O19	1.986(12)	P2–O20	1.536(13)
W6–O30	1.955(14)	W12–O5	2.364(13)	P2–O53	1.592(13)
W6–O18	2.010(13)	W13–O31	1.704(15)	C1–C2	1.496(10)
W6–O26	2.344(13)	W13–O56	1.876(14)	C2–C3	1.508(10)
W7–O24	1.711(14)	W13–O54	1.883(13)	C3–O57	1.292(10)
W7–O36	1.854(13)	W13–O37	1.947(14)	C3–O58	1.277(10)
Bond	**Angle(°)**	**Bond**	**Angle(°)**	**Bond**	**Angle(°)**
O4–W1–O39	167.3(5)	O36–W7–O23	161.4(6)	O56–W13–O53	73.2(5)
O25–W1–O17	172.0(5)	O41–W7–O20	73.2(5)	O54–W13–O53	73.8(5)
O11–W1–O17	73.3(5)	O23–W7–O20	78.1(5)	O43–W14–O54	158.3(6)

O39–W1–O17	80.9(5)	O35–W8–O8	161.4(5)	O33–W14–O53	167.7(6)
O8–W2–O43	160.7(6)	O46–W8–O5	172.7(6)	O42–W14–O53	72.0(5)
O49–W2–O14	171.9(6)	O35–W8–O5	80.3(5)	O54–W14–O53	73.1(5)
O51–W2–O14	72.6(5)	O12–W8–O5	73.2(5)	O22–W15–O56	157.1(6)
O43–W2–O14	78.9(5)	O29-W9-O20	170.1(6)	O32–W15–O53	169.0(6)
O19–W3–O22	161.8(6)	O21–W9–O45	161.9(5)	O42–W15–O53	71.6(5)
O7–W3–O14	172.0(6)	O41–W9–O20	73.6(5)	O56–W15–O53	72.4(5)
O51–W3–O14	73.2(5)	O45–W9–O20	79.6(5)	C1–Sn1–O27	177.5(7)
O22–W3–O14	79.4(5)	O38–W10–O16	171.0(6)	O35–Sn1–O52#1	158.9(5)
O1–W4–O17	169.7(6)	O55–W10–O21	163.6(5)	O39#1–Sn1–O27	76.4(5)
O40–W4–O50	165.3(6)	O15–W10–O16	71.2(5)	O52#1–Sn1–O27	76.5(5)
O11–W4–O17	71.8(5)	O21–W10–O16	80.7(5)	O40–Cu1–O27#1	175.1(6)
O50–W4–O17	81.3(5)	O37–W11–O4	161.2(6)	O55#1–Cu1–O27	176.2(5)
O23–W5–O52	166.0(6)	O48–W11–O26	171.3(6)	O39–Cu1–O27#1	76.4(5)
O13–W5–O16	169.4(6)	O30–W11–O26	73.4(5)	O52#1–Cu1–O27	77.2(5)
O15–W5–O16	72.7(5)	O4–W11–O26	78.4(5)	O16–P1–O5	112.4(7)
O52–W5–O16	79.6(5)	O3–W12–O19	163.6(6)	O16–P1–O17	111.6(7)
O50–W6–O18	162.7(5)	O28–W12–O5	175.4(6)	O5–P1–O17	111.5(7)
O44–W6–O26	170.0(6)	O3–W12–O5	81.3(5)	O14–P2–O26	111.4(8)
O30–W6–O26	73.5(5)	O12–W12–O5	73.9(5)	O14–P2–O20	113.2(7)
O18–W6–O26	79.4(5)	O54–W13–O37	155.7(6)	O26–P2–O20	112.1(8)
O24–W7–O20	170.8(5)	O31–W13–O53	174.5(7)		

Symmetry transformations used to generate equivalent atoms: #1 -x+1,-y,-z+1

Table S2 Selected bond lengths (Å) and angles (º) for SnR-Zn-P_2W_{15}

Bond	**Length (Å)**	**Bond**	**Length (Å)**	**Bond**	**Length (Å)**
W1–O41	1.723(12)	W7–O1	1.870(13)	W13–O7	1.945(11)
W1–O27	1.826(10)	W7–O39	1.967(11)	W13–O14	2.411(11)
W1–O42	1.911(11)	W7–O46	2.019(11)	W14–O24	1.702(13)
W1–O40	1.924(12)	W7–O10	2.341(10)	W14–O35	1.854(12)
W1–O35	2.003(11)	W8–O2	1.715(11)	W14–O44	1.857(11)
W1–O56	2.391(11)	W8–O38	1.771(11)	W14–O52	1.924(11)
W2–O9	1.729(12)	W8–O30	1.877(11)	W14–O53	1.992(13)
W2–O12	1.827(10)	W8–O4	1.961(10)	W14–O14	2.350(10)
W2–O45	1.889(10)	W8–O50	2.059(10)	W15–O25	1.698(12)
W2–O42	1.901(11)	W8–O15	2.379(10)	W15–O36	1.864(11)
W2–O34	1.983(10)	W9–O49	1.692(11)	W15–O34	1.865(11)
W2–O56	2.363(10)	W9–O50	1.813(10)	W15–O52	1.946(11)
W3–O22	1.711(13)	W9–O45	1.884(11)	W15–O51	1.974(13)
W3–O20	1.835(10)	W9–O37	1.941(11)	W15–O14	2.358(10)
W3–O4	1.871(10)	W9–O36	1.997(11)	Sn1–O5	2.045(11)
W3–O3	1.886(10)	W9–O11	2.342(10)	Sn1–O26	2.054(10)
W3–O43	2.072(11)	W10–O19	1.696(11)	Sn1–O43#1	2.064(11)
W3–O15	2.354(11)	W10–O5	1.821(11)	Sn1–O29#1	2.089(11)
W4–O16	1.708(12)	W10–O8	1.897(11)	Sn1–C1	2.12(2)
W4–O26	1.811(10)	W10–O30	1.920(11)	Sn1–O55	2.300(11)

W4–O1	1.911(13)	W10–O12	1.973(10)	Zn1–O33#1	2.028(11)
W4–O8	1.927(11)	W10–O28	2.367(10)	Zn1–O38	2.030(11)
W4–O27	1.973(10)	W11–O18	1.699(12)	Zn1–O29#1	2.073(11)
W4–O28	2.381(11)	W11–O7	1.868(11)	Zn1–O43	2.104(12)
W5–O32	1.682(12)	W11–O37	1.883(10)	Zn1–O55#1	2.225(11)
W5–O17	1.830(10)	W11–O48	1.885(10)	Zn1–O55	2.250(12)
W5–O39	1.874(10)	W11–O20	1.944(10)	P1–O15	1.513(10)
W5–O3	1.918(10)	W11–O11	2.371(11)	P1–O28	1.513(11)
W5–O29	2.056(10)	W12–O23	1.714(11)	P1–O10	1.521(11)
W5–O10	2.357(10)	W12–O46	1.824(11)	P1–O55	1.608(11)
W6–O31	1.680(12)	W12–O40	1.845(12)	P2–O56	1.506(11)
W6–O47	1.862(11)	W12–O6	1.937(11)	P2–O11	1.514(11)
W6–O6	1.904(11)	W12–O44	2.000(11)	P2–O13	1.526(11)
W6– O48	1.908(10)	W12–O13	2.341(10)	P2–O14	1.576(11)
W6–O17	1.947(10)	W13–O21	1.717(12)	C1–C2	1.518(10)
W6–O13	2.366(11)	W13–O53	1.851(12)	C2–C3	1.525(10)
W7–O54	1.737(11)	W13–O51	1.879(12)	C3–O57	1.276(10)
W7–O33	1.797(11)	W13–O47	1.941(11)	C3 –O58	1.292(10)
Bond	**Angle(°)**	**Bond**	**Angle(°)**	**Bond**	**Angle(°)**
O41–W1–O56	171.1(5)	O33–W7–O46	164.3(5)	O51–W13–O14	73.7(4)
O27–W1–O35	161.2(5)	O46–W7–O10	80.8(4)	O53–W13–O14	73.8(4)
O35–W1–O56	79.4(4)	O39–W7–O10	72.3(4)	O24–W14–O14	168.7(5)
O42–W1–O56	72.8(4)	O2–W8–O15	170.7(5)	O35–W14–O53	158.3(5)
O9–W2–O56	172.0(5)	O38–W8–O50	166.0(5)	O53–W14–O14	72.9(4)
O12–W2–O34	162.6(5)	O50–W8–O15	81.9(4)	O52–W14–O14	71.5(4)
O34–W2–O56	80.0(4)	O4–W8–O15	72.0(4)	O25–W15–O14	168.9(5)
O42–W2–O56	73.6(4)	O49–W9–O11	170.6(5)	O34-W15–O51	158.4(5)
O22–W3–O15	171.6(5)	O50–W9–O36	163.0(5)	O51–W15–O14	73.4(4)
O20–W3–O43	167.3(5)	O36–W9–O11	79.2(4)	O52–W15–O14	71.0(4)
O43–W3–O15	80.3(4)	O37–W9–O11	73.1(4)	O26–Sn1–O29#1	158.7(4)
O4–W3–O15	74.1(4)	O19–W10–O28	174.9(5)	C1–Sn1–O55	176.3(6)
O16–W4–O28	173.8(5)	O5–W10–O12	163.1(5)	O43#1–Sn1–O55	75.9(4)
O26–W4–O27	161.1(5)	O5–W10–O28	81.0(4)	O29#1–Sn1–O55	76.9(4)
O26–W4–O28	80.3(4)	O8–W10–O28	73.8(4)	O33#1–Zn1–O55	176.5(5)
O8–W4–O28	72.9(4)	O18–W11–O11	172.4(5)	O38–Zn1–O55#1	175.1(4)
O32–W5–O10	170.0(5)	O7–W11–O20	161.1(5)	O43–Zn1–O55#1	76.8(4)
O17–W5–O29	166.1(5)	O20–W11–O11	78.3(4)	O29#1–Zn1–O55	78.3(4)
O29–W5–O10	79.8(4)	O37–W11–O11	73.4(4)	O15–P1–O28	111.9(6)
O39–W5–O10	73.4(4)	O23–W12–O13	170.7(5)	O15–P1–O10	111.6(6)
O31–W6–O13	171.9(5)	O46–W12–O44	162.2(4)	O28–P1–O10	111.5(6)
O47–W6–O17	161.3(5)	O44–W12–O13	79.6(4)	O56–P2–O11	112.5(6)
O17–W6–O13	77.8(4)	O6–W12–O13	73.4(4)	O56–P2–O13	112.0(6)
O6–W6–O13	73.4(4)	O21–W13–O14	174.8(5)	O11–P2–O13	111.2(6)
O54–W7–O10	170.8(5)	O51–W13–O47	155.8(5)		

Symmetry transformations used to generate equivalent atoms: #1 -x,-y,-z+1

Table S3 Hydrogen bonds for SnR-Cu-P_2W_{15}

D–H...A	d(D–H) (Å)	d(H...A) (Å)	d(D...A) (Å)	<(DHA) (°)
N1–H1C...O11#2	0.86	2.10	2.94(2)	163.3
N1–H1D...O33#3	0.86	2.02	2.88(3)	177.4
N2–H2C...O1#2	0.86	2.18	3.04(2)	172.3
N2–H2D...O15#1	0.86	2.09	2.92(2)	161.5
N3–H3A...O13#1	0.86	2.22	3.07(2)	169.5
N3–H3B...O42#3	0.86	2.15	2.98(2)	162.1
N4–H4A...O43#4	0.86	2.21	3.06(3)	167.9
N4–H4B...O30	0.86	1.98	2.82(2)	166.6
N5–H5A...O22#4	0.86	2.12	2.90(3)	149.0
N5–H5A...O51#4	0.86	2.59	3.23(3)	131.9
N5–H5B...O24#5	0.86	2.14	2.97(3)	162.4
N6–H6A...O41#5	0.86	2.08	2.91(3)	164.5
N6–H6B...O44	0.86	2.04	2.89(2)	171.1
N7–H7A...O29	0.86	2.32	3.12(3)	155.8
N7–H7B...O7#6	0.86	2.58	3.32(3)	144.5
N8–H8B...O29	0.86	2.55	3.31(4)	148.1
N8–H8B...O10	0.86	2.64	3.34(3)	139.2
N9–H9A...O31#7	0.86	2.27	3.13(3)	171.5
N9–H9B...O7#6	0.86	2.22	3.05(3)	162.4
N10–H10B...O38	0.86	2.37	3.10(3)	142.9
N10–H10B...O2	0.86	2.64	3.38(3)	144.2
N11–H11A...O47#6	0.86	2.28	3.10(3)	157.9
N11–H11B...O38	0.86	2.13	2.92(3)	152.5
N12–H12A...O28#6	0.86	2.21	3.01(3)	153.6
N13–H13A...O48	0.86	2.34	3.11(3)	148.6
N13–H13A...O33#4	0.86	2.64	3.08(3)	112.8
N13–H13B...O1W#8	0.86	2.54	3.31(4)	148.3
N13–H13B...O45#4	0.86	2.59	3.22(3)	130.7
N14–H14A...O32#9	0.86	2.21	3.00(3)	153.0
N14–H14B...O34	0.86	2.35	3.11(3)	146.6
N15–H15A...O32#9	0.86	2.44	3.16(4)	142.2
N15–H15B...O1W#8	0.86	2.54	3.31(4)	149.5
N16–H16A...O55#1	0.86	2.41	3.16(3)	144.6
N16–H16A...O35#1	0.86	2.52	3.19(3)	136.0
N17–H17A...O55#1	0.86	2.36	3.11(3)	144.9
N17–H17B...O1#2	0.86	2.43	3.03(3)	127.3
N18–H18B...O2W#2	0.86	1.91	2.76(4)	169.0

Symmetry transformations used to generate equivalent atoms:#1 -x+1,-y,-z+1; #2 -x,-y,-z+1; #3 -x+1/2,y-1/2,-z+3/2; #4 x-1/2,-y+1/2,z-1/2; #5 x-1,y,z; #6 x+1,y,z;#7 x+1/2,-y+1/2,z+1/2; #8 x,y,z-1; #9 x+1/2,-y+1/2,z-1/2

Table S4 Hydrogen bonds for SnR-Zn-P_2W_{15}

D–H...A	d(D–H) (Å)	d(H...A) (Å)	d(D...A) (Å)	<(DHA)(Å)
N1–H1A...O21	0.86	2.27	3.12(2)	169.3
N1–H1B...O9#2	0.86	2.14	2.98(2)	163.9
N2–H2B...O23#3	0.86	2.45	3.22(3)	150.2
N2–H2B...O40#3	0.86	2.60	3.29(3)	137.5
N3–H3A...O23#3	0.86	2.26	3.06(3)	155.9
N3–H3B...O9#2	0.86	2.63	3.35(2)	142.2
N4–H4A...O18#4	0.86	2.45	3.14(3)	137.1
N4–H4A...O24	0.86	2.58	3.08(2)	118.1
N4–H4B...O2W	0.86	2.44	3.22(3)	150.7
N4–H4B...O44	0.86	2.62	3.22(2)	128.2
N5–H5A...O48#4	0.86	2.30	3.07(2)	149.4
N5–H5B...O25#5	0.86	2.18	2.99(3)	156.8
N6–H6A...O25#5	0.86	2.49	3.20(3)	141.3
N6–H6B...O2W	0.86	2.45	3.22(4)	150.1
N7–H7A...O19#5	0.86	2.26	3.01(3)	145.8
N8–H8A...O30#5	0.86	2.29	3.10(2)	156.3
N8–H8B...O54	0.86	2.07	2.88(2)	156.7
N9–H9B...O54	0.86	2.38	3.11(3)	142.9
N9–H9A...O5W	0.86	2.37	3.16(8)	151.9
N10–H10A...O31	0.86	2.16	2.983(19)	160.4
N10–H10B...O34#2	0.86	2.13	2.90(2)	148.3
N10–H10B...O42#2	0.86	2.56	3.21(2)	133.4
N11–H11A...O37#5	0.86	1.97	2.822(18)	170.3
N11–H11B...O35#2	0.86	2.15	3.00(2)	170.2
N12–H12B...O49#5	0.86	2.08	2.94(2)	175.7
N12–H12A...O6	0.86	2.05	2.90(2)	169.0
N13–H13A...O4	0.86	2.13	2.936(18)	156.1
N13–H13B...O24#3	0.86	2.04	2.90(2)	176.0
N14–H14A...O32#6	0.86	2.23	3.06(2)	161.8
N14–H14B...O52#3	0.86	2.19	3.01(2)	159.7
N15–H15A...O39#6	0.86	2.04	2.890(19)	167.8
N15–H15B...O2	0.86	2.18	3.02(2)	168.6
N16–H16B...O33	0.86	2.37	3.13(3)	147.3
N16–H16B...O26	0.86	2.52	3.20(3)	135.8
N17–H17A...O2#5	0.86	2.44	3.02(3)	125.7
N17–H17B...O33	0.86	2.25	3.05(3)	154.3
N18–H18A...O1W#7	0.86	1.93	2.79(4)	174.6

Symmetry transformations used to generate equivalent atoms:#1-x,-y,-z+1; #2 x+1/2,-y+1/2,z-1/2; #3 x-1/2,-y+1/2,z-1/2; #4 x+1/2,-y+1/2,z+1/2; #5 x+1,y,z; #6 x-1,y,z; #7 -x+1,-y,-z+1

3. Chemical and Physical characterizations

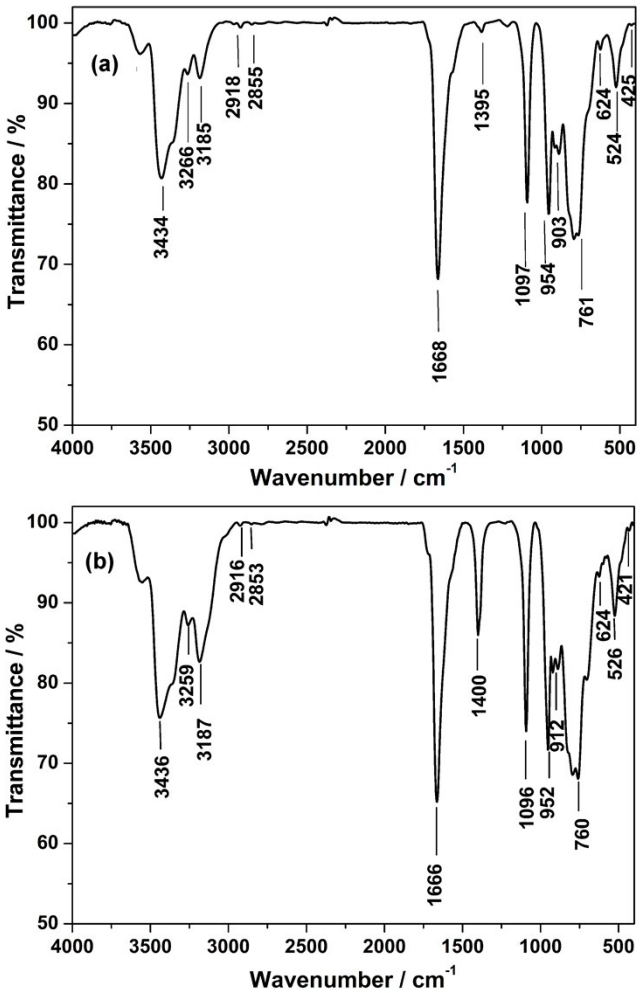

Fig. S4. IR spectra of SnR-Cu-P_2W_{15} (a) and SnR-Zn-P_2W_{15} (b)

IR spectra of SnR-Cu-P_2W_{15} and SnR-Zn-P_2W_{15} recorded between 4000 and 400 cm^{-1} with KBr pellet are similar: the peaks at 1097–760 cm^{-1} can be attributed to the characteristic vibrations of the POM skeleton; the bands at 1097 or 1096, 954 or 952, 903 or 912 and 761or 760 cm^{-1} are attributed to ν(P–O_a), ν(W=O_d), ν(W–O_b) and ν(W–O_c)[S1] (O_a,O_b/O_c and O_d represent tetrahedral, bridging and terminal O atoms), respectively. The appearance of a peak at 425or 421 cm^{-1} may be due to the symmetric vibration of the Sn–C bond. The observed overlapped peak at 524 or 526 cm^{-1} may be caused by ν(Cu–O) or ν(Zn–O) and the antisymmetric vibration of the Sn–C bond. A broad band due to lattice water molecules is located at 3434 or 3436 cm^{-1}. The ν(N–H) peaks lie in the 3266–3185 or 3259–3187 cm^{-1} region. The peaks at 2918(or 2916) and 2855 (or 2853) cm^{-1} are ascribed to the stretching vibration of the organic group –CH_2, while the sharp peaks at 1668 (or 1666) and 1395 (or 1400) cm^{-1} are attributed to the stretching vibration of –COO. All the results indicate the presence of the carboxyethyltin group and the POM framework in SnR-Cu-P_2W_{15} and SnR-Zn-P_2W_{15}, which is in good agreement with the single crystal structural analysis.

[S1] T. T. Yu, H. Y. Ma, C. J. Zhang, H. J. Pang, S. B. Li, H. Liu, *Dalton Trans.* **2013**, *42*, 16328.

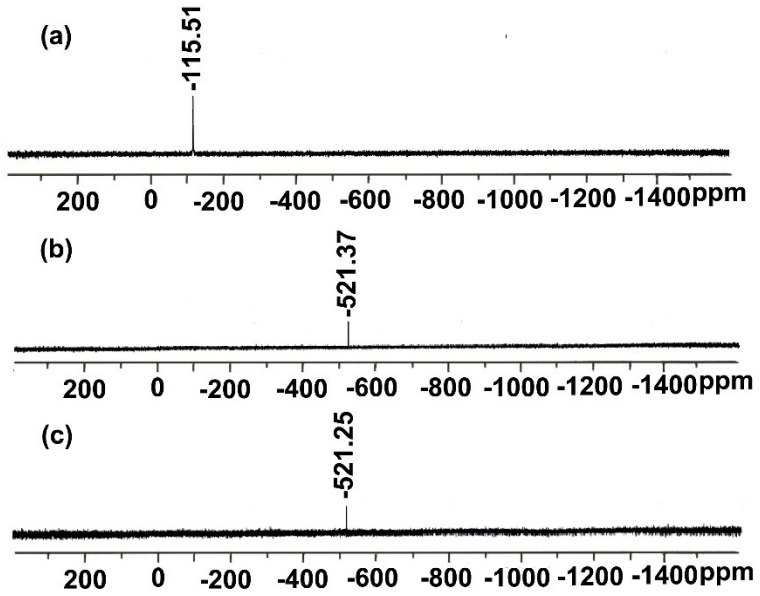

Fig. S5. The ^{119}Sn NMR spectra of $Cl_3Sn(CH_2)_2COOCH_3$ (a), SnR-Cu-P_2W_{15} (b) and SnR-Zn-P_2W_{15} (c)

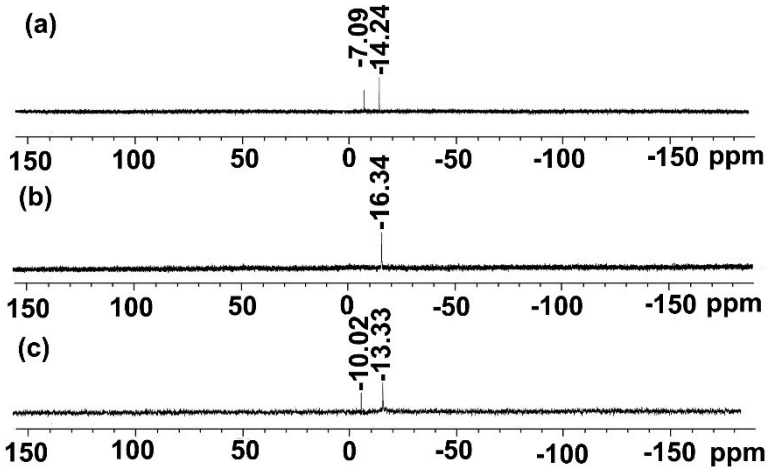

Fig. S6. The ^{31}P NMR spectra of P_2W_{15} (a), Cu-P_2W_{15} (b) and SnR-Cu-P_2W_{15} (c)

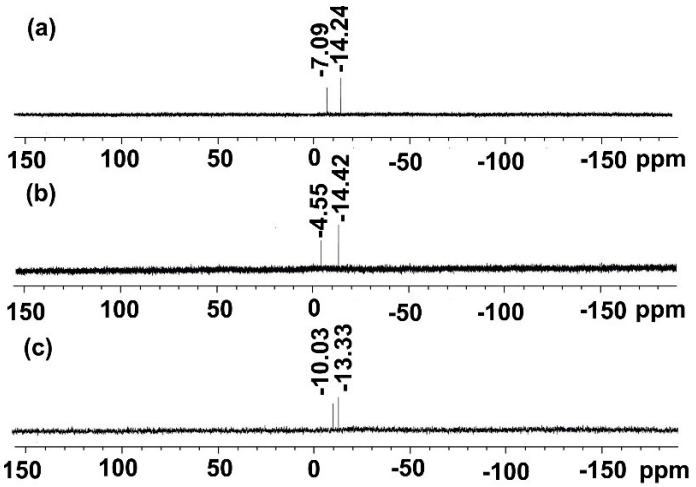

Fig. S7. The ^{31}P NMR spectra of P_2W_{15} (a), Zn-P_2W_{15} (b) and SnR-Zn-P_2W_{15} (c)

The ^{119}Sn and ^{31}P NMR spectra for SnR-Cu-P_2W_{15}, SnR-Zn-P_2W_{15} and starting materials $Cl_3Sn(CH_2)_2COOCH_3$, Cu-P_2W_{15}, Zn-P_2W_{15} and P_2W_{15} were indicated to further confirm the organotin group was introduced into the POM skeleton and obtain more perfect sandwich-type structural information. As seen in Fig. S5, the chemical shit of ^{119}Sn for the precursor $Cl_3Sn(CH_2)_2COOCH_3$ ($CDCl_3$/$(CH_3)_4Sn$) is at δ = −115.51 ppm, while the ^{119}Sn NMR chemical shifts of SnR-Cu-P_2W_{15} and SnR-Zn-P_2W_{15} shifts to high field (δ =−521.37 ppm and−521.25 ppm) due to the increased electron density on tin atom, indicating of organotin groups into the P_2W_{15} skeleton. The ^{31}P NMR spectra of SnR-Cu-P_2W_{15} showed two intense peaks at δ =−10.02 and −13.33 ppm (Fig. S6c). Meantime, the ^{31}P NMR spectra of SnR-Zn-P_2W_{15}also showed two intense peaks at δ =−10.03 and −13.33 ppm (Fig. S7c), which are consistent with the peaks observed for P_2W_{15}located at δ = −7.09 and −14.24 ppm (Fig. S6a), indicating that the phosphorous atoms are in two diverse chemical environments. In addition, ^{31}P NMR spectrum for Cu-P_2W_{15} (δ = −16.42 ppm) exhibits only one intense single peak (Fig. S6b), which was probably influenced by the four incorporated paramagnetic Cu^{2+} ions.

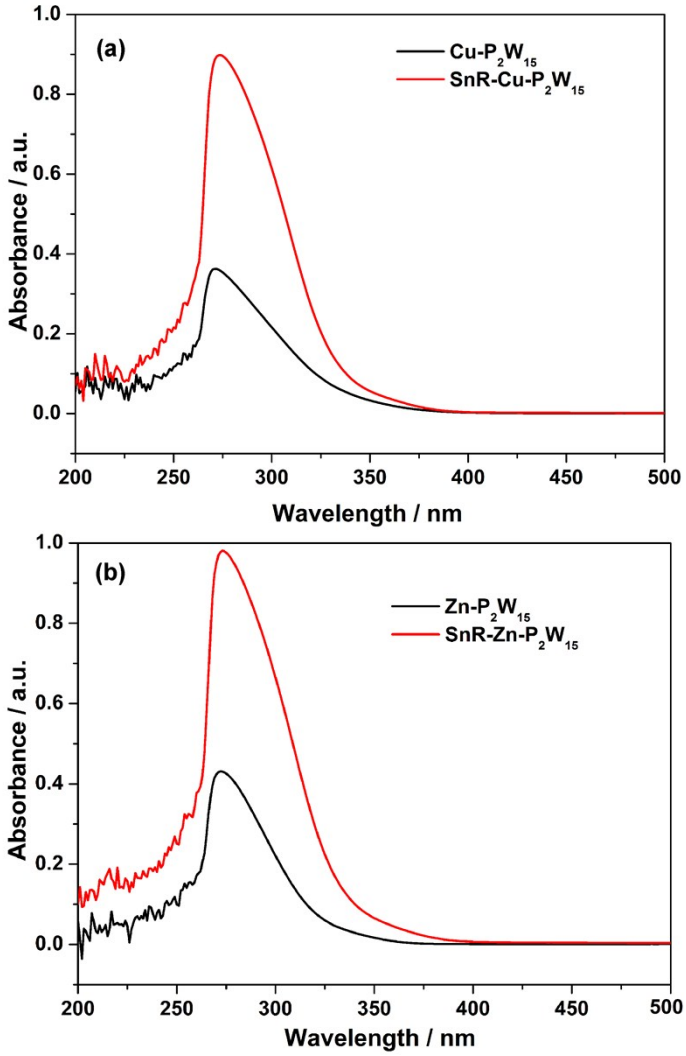

Fig. S8. UV/Vis absorption spectra of SnR-Cu-P_2W_{15} and Cu-P_2W_{15} (a); SnR-Zn-P_2W_{15} and Zn-P_2W_{15} (b) in aqueous solution, respectively

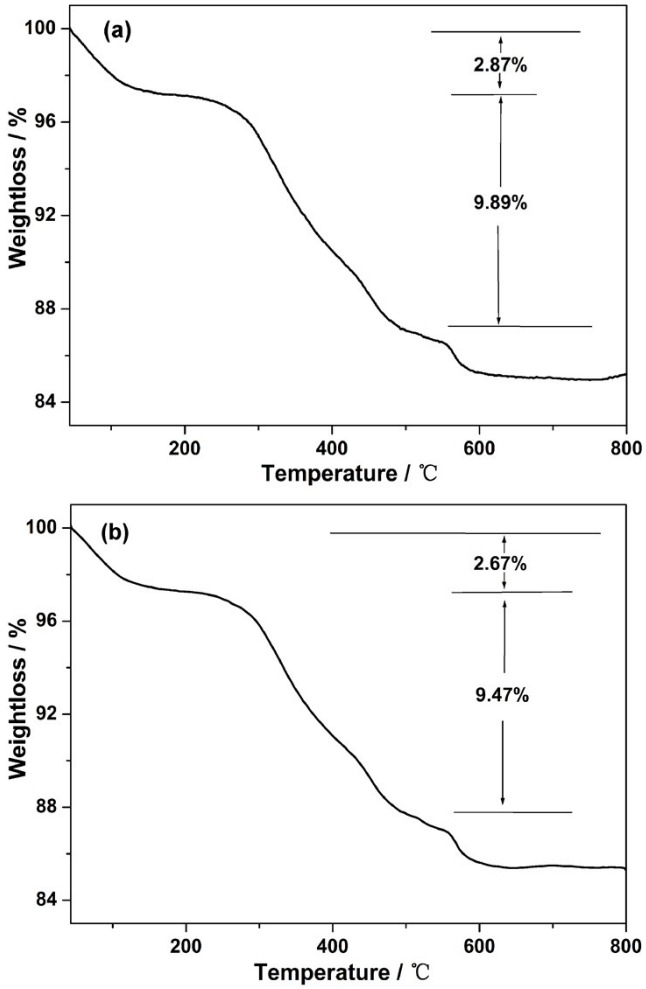

Fig. S9. TG curves of SnR-Cu-P_2W_{15} (a) and SnR-Zn-P_2W_{15} (b)

In order to investigate thermal stabilities of SnR-Cu-P_2W_{15} and SnR-Zn-P_2W_{15}, thermal gravimetric (TG) analyses were measured and TG curves are plotted in Fig. S9. SnR-Cu-P_2W_{15}shows a three-continuous weightloss from 42 to 800 °C (Fig. S9a). The first weight loss of 2.87% (calcd 2.83%)was observed below 200 °C, corresponding to the loss of all crystal water molecules. The second weight loss of 9.89% (calcd 9.75%) in the temperature range of 200-490 °C corresponds to the removal of twelve $[C(NH_2)_3]^+$ organic cations and four H^+ ions, as well as two $C_3H_4O_2$ groups. In addition, the compound continuously lost weight at temperatures higher than 490 °C, which is mainly attributed to the loss of phosphorus oxide species that are easily to sublimate. For SnR-Zn-P_2W_{15}, it has similar thermal stability to SnR-Cu-P_2W_{15}. In the range of 42 to 800 °C, a three-continuous weight loss step is also observed. The first weight loss of 2.67% (calcd 2.65%) occurred at 42-200 °C, and corresponds to the loss of all lattice water molecules. The second weight loss of 9.47% (calcd9.16%) in the temperature range of 200-490 °C correspond to the removal of eleven $[C(NH_2)_3]^+$ organic cations and five H^+ ions, as well as two $C_3H_4O_2$ groups. In addition, the compound continuously lost weight at temperatures higher than 490 °C, which is mainly attributed to the loss of phosphorus oxide species that are easily to sublimate.

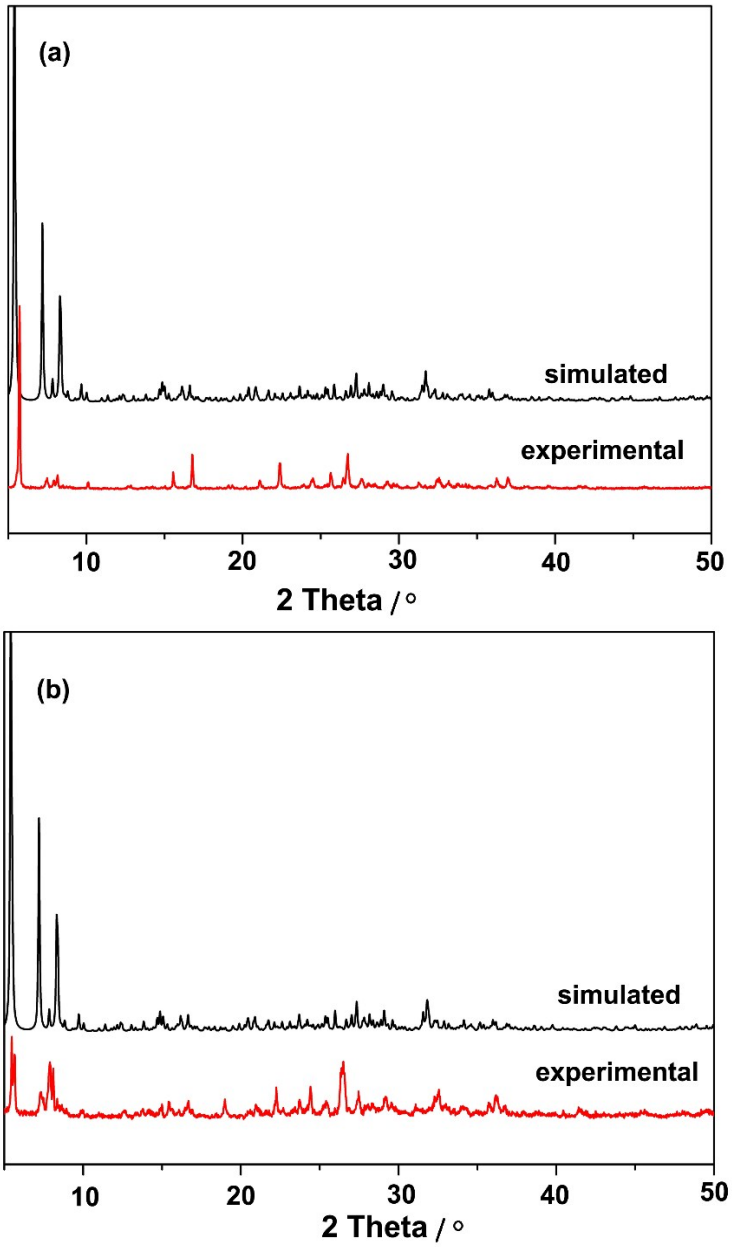

Fig. S10. The simulated and experimental XRPD patterns of compounds SnR-Cu-P_2W_{15} (a) and SnR-Zn-P_2W_{15} (b), respectively

The purity of the as-synthesized compounds were evaluated by XRPD patterns for experimental and simulated results of SnR-Cu-P_2W_{15} and SnR-Zn-P_2W_{15} in Fig. S10, which illustrated the diffraction peaks of two patterns match well, indicating its good phase purity. The difference of intensity is probably due to the variation in preferred orientation of the powder sample during collection of the experimental XRPD pattern.

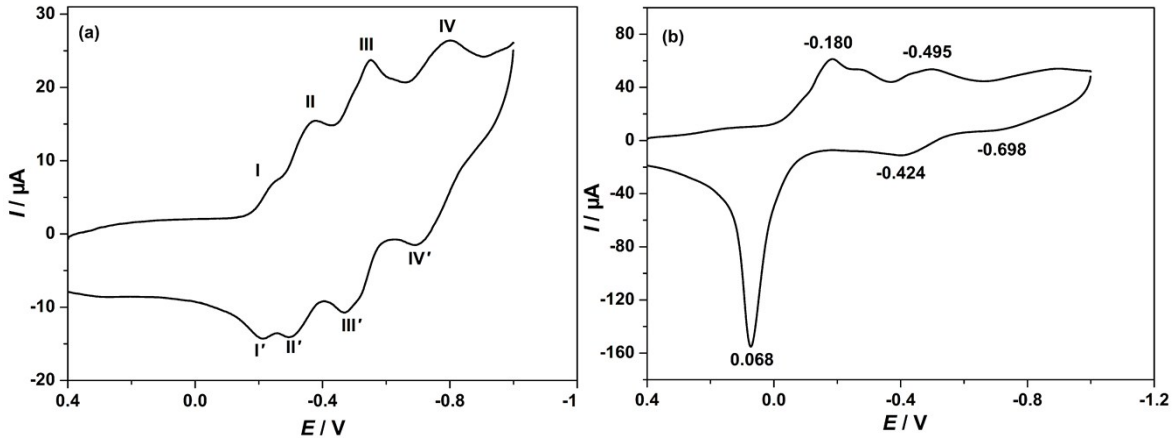

Fig. S11. Cyclic voltammograms of SnR-Cu-P_2W_{15} (a) andCu-P_2W_{15} (b) in 1 mol L^{-1} Na_2SO_4-H_2SO_4 (pH = 4) aqueous solutions at the scan rate of 50 mV s^{-1}

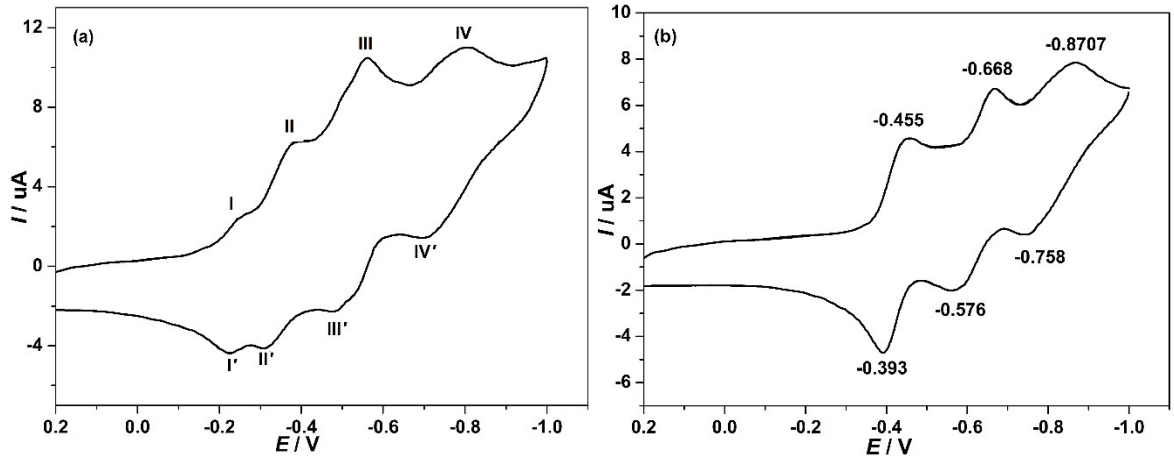

Fig. S12. Cyclic voltammograms of SnR-Zn-P_2W_{15} (a) and Zn-P_2W_{15} (b) in 1 mol L^{-1} Na_2SO_4-H_2SO_4 (pH = 4) aqueous solutions at the scan rate of 50 mV s^{-1}

The electrochemical behavior was conducted with cyclic voltammetric (CV) method in 1 mol L^{-1} Na_2SO_4-H_2SO_4 (pH = 4) aqueous solutions at the scan rate of 50 mV s^{-1} at room temperature. In the CV curve of Cu-P_2W_{15} (Fig. S11b), the peak at 0.068V is assigned to the redox process of Cu^0/Cu^{2+}.[S2] Different from Cu-P_2W_{15}, SnR-Cu-P_2W_{15}(Fig. S11a) show four continuous reversible redox waves located at -0.235 and -0.208 V (I-I′), -0.374 and -0.296 V (II–II′), -0.550 and -0.468 V(III–III′), and -0.799 and -0.688 V(IV–IV′) with peak potential separations (Δ*E*p) of 0.027, 0.078, 0.082 and 0.111V, respectively, which can be attributed to the electrochemical response of W centers.[S3] Although differing from its parent POM Zn-P_2W_{15},SnR-Zn-P_2W_{15} shows similar electrochemical behavior with SnR-Cu-P_2W_{15}, and was characterized by four continuous redox steps located at −0.235 and −0.226 V (I–I′), −0.381 and −0.310 V (II–II′), −0.556 and −0.485 V (III–III′) and −0.803 and −0.711 V(IV–IV′), with their corresponding peak potential separations (Δ*E*p) of 0.09, 0.071, 0.071 and 0.092 V, respectively (Fig. S12a).

[S2] B. Keita, I. M. Mbomekalle, L. Nadjo, *Electrochem. Commun.* 2003, **5**, 830.

[S3] J. P. Bai, F. Su, H. T. Zhu, H. Sun, L. C. Zhang, M. Y. Liu, W. S. You, Z. M. Zhu, *Dalton Trans.* 2015, **44**, 6423.

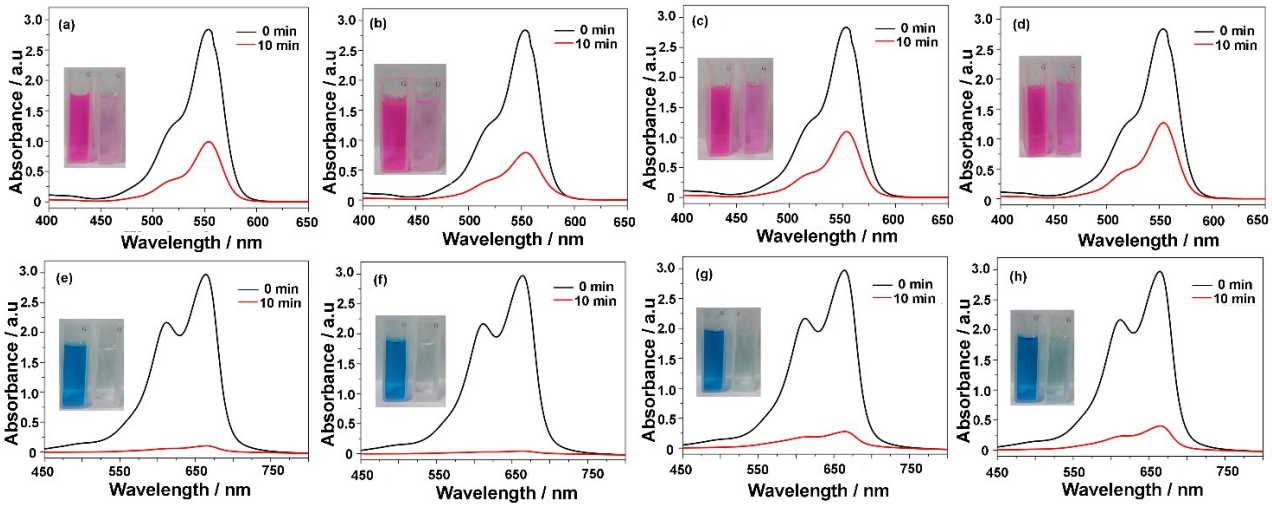

Fig. S13. UV/Vis curves of RhB/MB solution in diluted 60 fold before and after the adsorption of SnR-M-P_2W_{15} (M= Mn (a,e); Co (b, f); Cu (c, g); Zn (d, h)) for 10 min. Inset: the color change of the dye solution before and after adsorption experiments

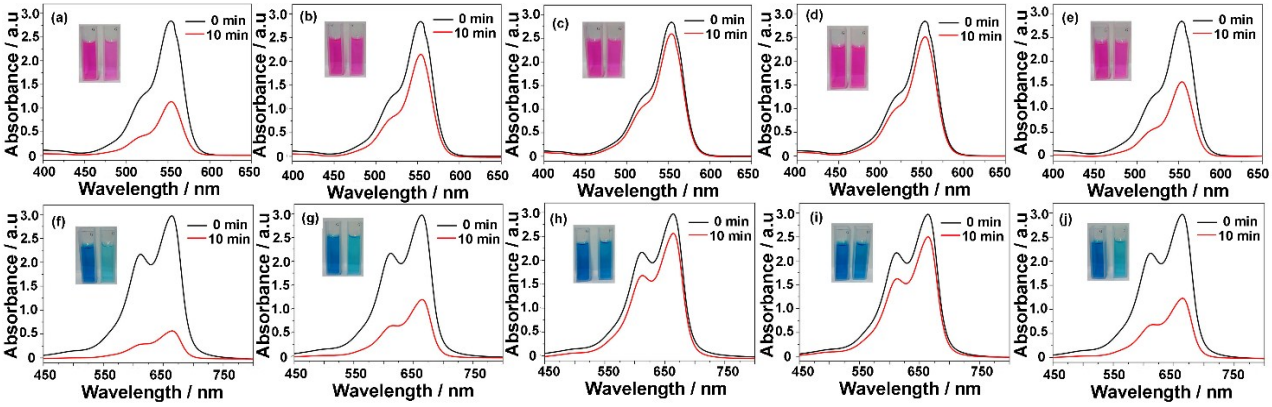

Fig. S14. UV/Vis curves of RhB/MB solution in diluted 60 fold before and after the adsorption of (M= Mn (a, f); Co (b, g); Cu (c, h); Zn (d, i)) and P_2W_{15} (e, j) for 10 min. Inset: the color change of the dye solution before and after adsorption experiments

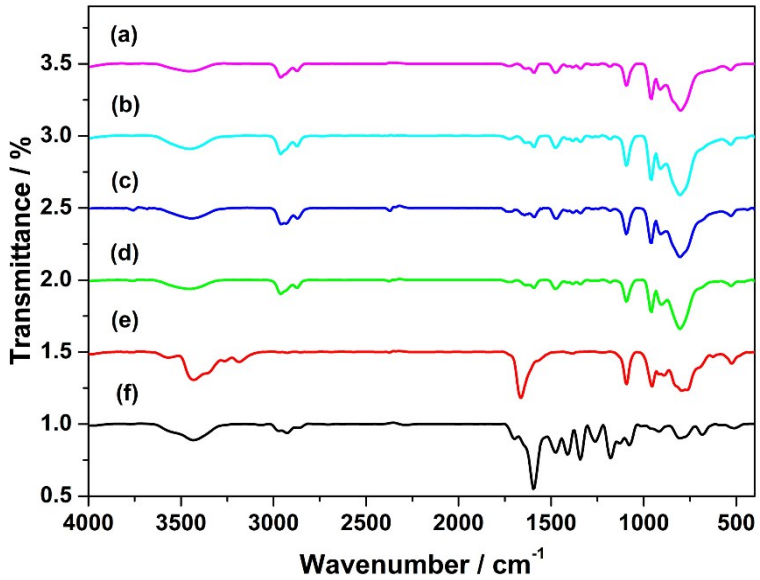

Fig. S15. FTIR spectra of SnR-M-P_2W_{15}/RhB composite materials (M= Mn (a), Co (b), Cu (c), Zn (d)), pure SnR-Cu-P_2W_{15} (e) and pure RhB (f)

Fig. S15 shows the FTIR spectra of SnR-M-P_2W_{15}/RhB(M=Mn, Co, Cu, Zn) composite materials. Compared to FTIR spectra of pure SnR-Cu-P_2W_{15} (Fig. S15e) and RhB (Fig. S15f), the bands at 1096, 960, 912 and 797 cm^{-1} for SnR-Cu-P_2W_{15}/RhB composite are due to the characteristic peak $\nu(P–O_a)$, $\nu(W=O_d)$, $\nu(W–O_b)$ and $\nu(W–O_c)$, respectively, while the peaks between 1597 and 1133 cm^{-1} are ascribed to the stretching vibration of the organic group of RhB. Also, the peaks located at 2963 and 2874 cm^{-1} are assigned to the C–H vibration of RhB. The results indicate that both SnR-M-P_2W_{15} (M=Mn, Co, Cu, Zn) and RhB maintain their stable structures after composition.

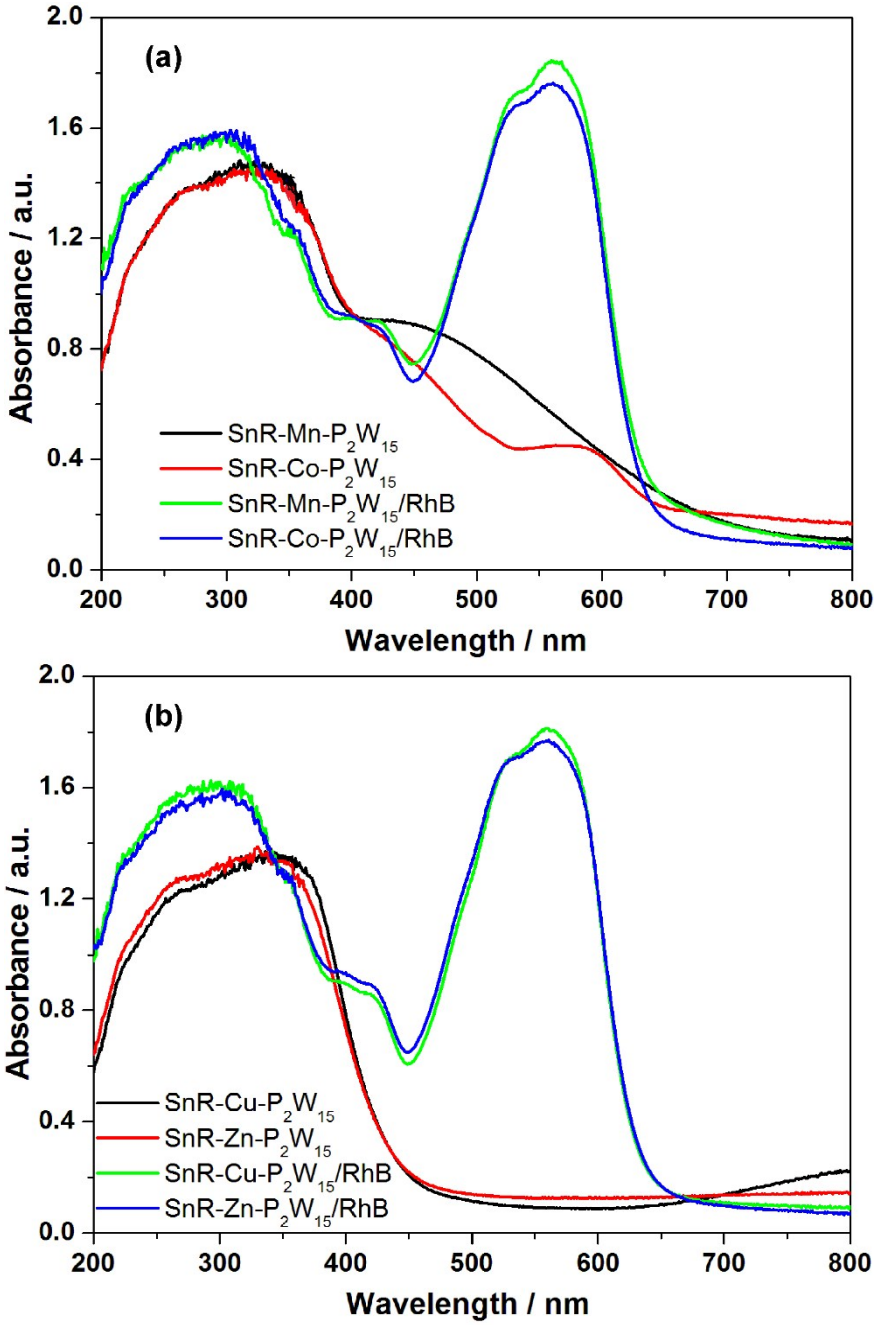

Fig. S16. Solid UV/Vis absorption spectra of SnR-M-P_2W_{15}/RhB composite materials and pure SnR-M-P_2W_{15} (M = Mn, Co) (a), and SnR-M-P_2W_{15}/RhB composite materials and pure SnR-M-P_2W_{15} (M = Cu, Zn) (b)

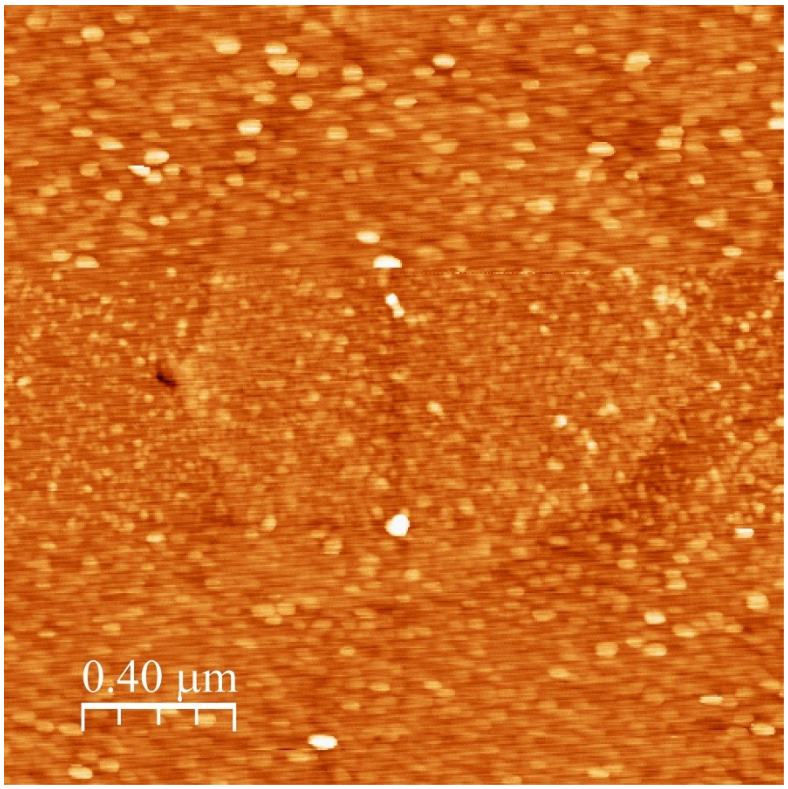

Fig. S17. Tapping mode AFM image of $(Co\text{-}P_2W_{15}/RhB)_4$ film on the silicon wafer

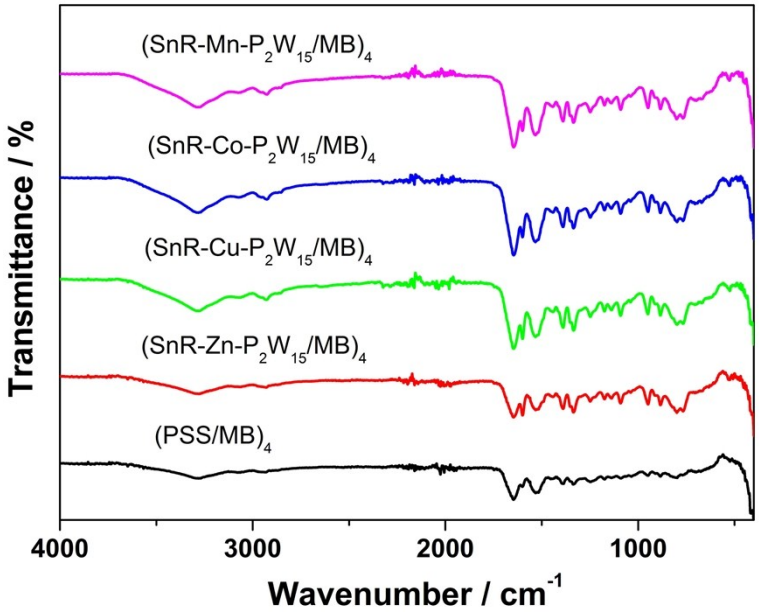

Fig. S18. FTIR spectra of $(SnR\text{-}M\text{-}P_2W_{15}/MB)_4$ (M=Mn, Co, Cu, Zn) and $(PSS/MB)_4$ films on CaF_2 substrate

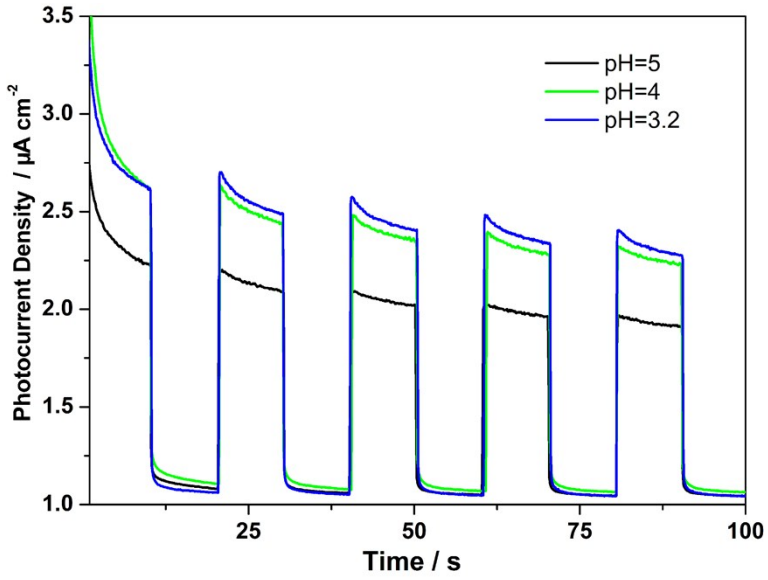

Fig. S19. Visible-light photocurrent responses for (SnR-Co-P_2W_{15}/RhB)$_4$ film prepared from SnR-Co-P_2W_{15} solution at different pH adjusted by HCl or NaOH solution with light on/off under irradiation (λ> 420 nm) in 0.1 mol L^{-1} Na_2SO_4 aqueous solution; the applied bias voltage: 0.5 V *vs* Ag/AgCl

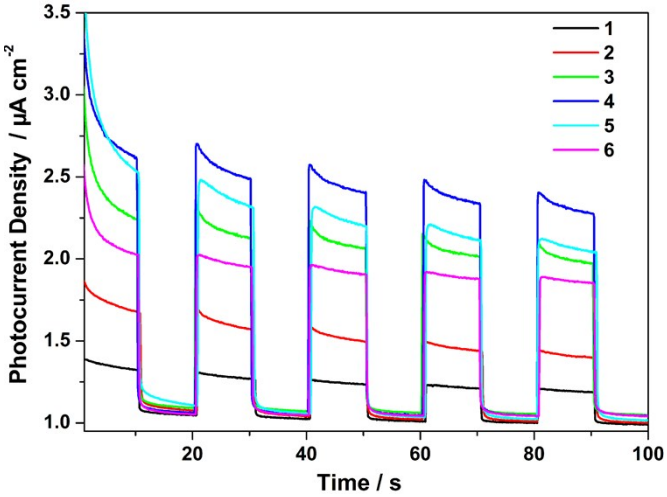

Fig. S20. Visible-light photocurrent responses for (SnR-Co-P_2W_{15}/RhB)$_n$ (n=1-6)films with light on/off under irradiation (λ> 420 nm) in 0.1 mol L^{-1} Na_2SO_4 aqueous solution; the applied bias voltage: 0.5 V *vs* Ag/AgCl

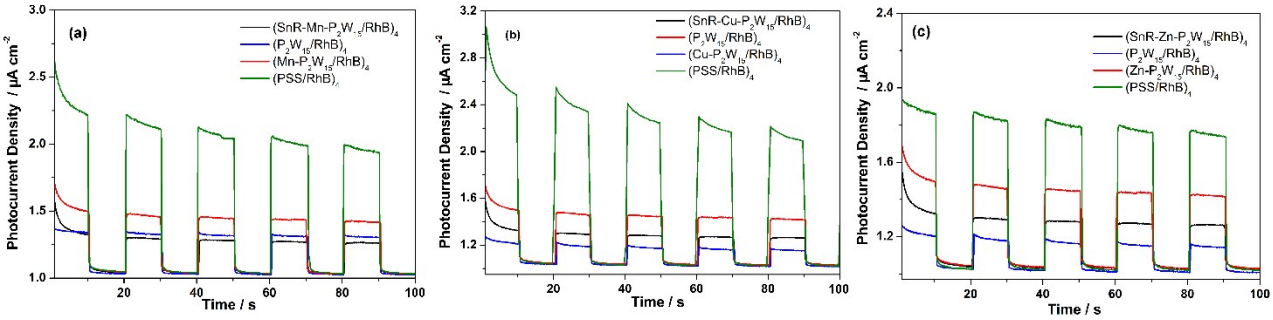

Fig. S21. Visible-light photocurrent responses for (SnR-M-P_2W_{15}/RhB)$_4$, (M-P_2W_{15}/RhB)$_4$, (P_2W_{15}/RhB)$_4$, and (PSS/RhB)$_4$ (M=Mn (a), Cu (b), Zn (c)) films with light on/off under irradiation (λ> 420 nm) in 0.1 mol L^{-1} Na_2SO_4 aqueous solution; the applied bias voltage: 0.5 V *vs* Ag/AgCl

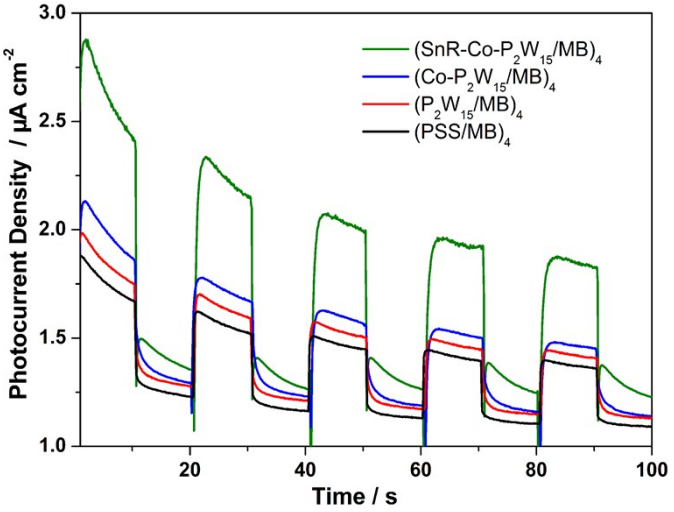

Fig. S22. Visible-light photocurrent responses for $(SnR\text{-}Co\text{-}P_2W_{15}/MB)_4$, $(Co\text{-}P_2W_{15}/MB)_4$, $(P_2W_{15}/MB)_4$ and $(PSS/MB)_4$ films with light on/off under irradiation (λ> 420 nm) in 0.1 mol L^{-1} Na_2SO_4 aqueous solution; the applied bias voltage: 0.5 V *vs* Ag/AgCl

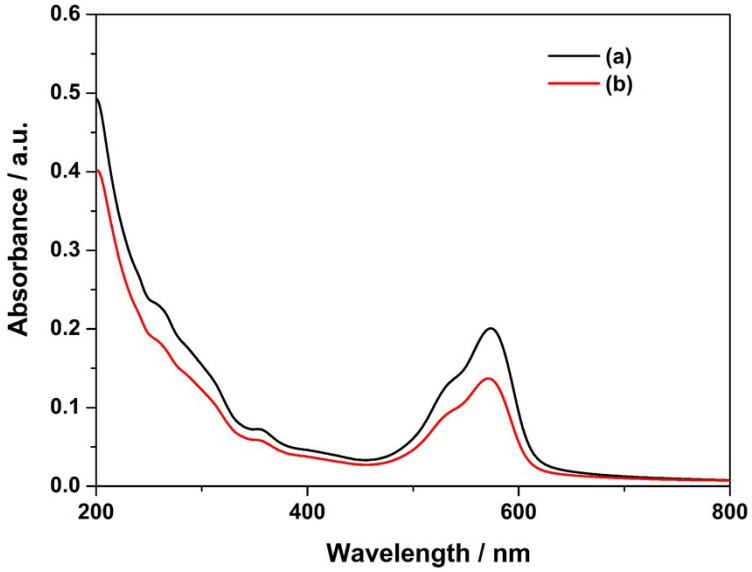

Fig. S23. UV/Vis absorption spectra of $(SnR\text{-}Co\text{-}P_2W_{15}/RhB)_4$ film on quartz plate before (a) and after (b) dipping in aqueous solution for 2 h

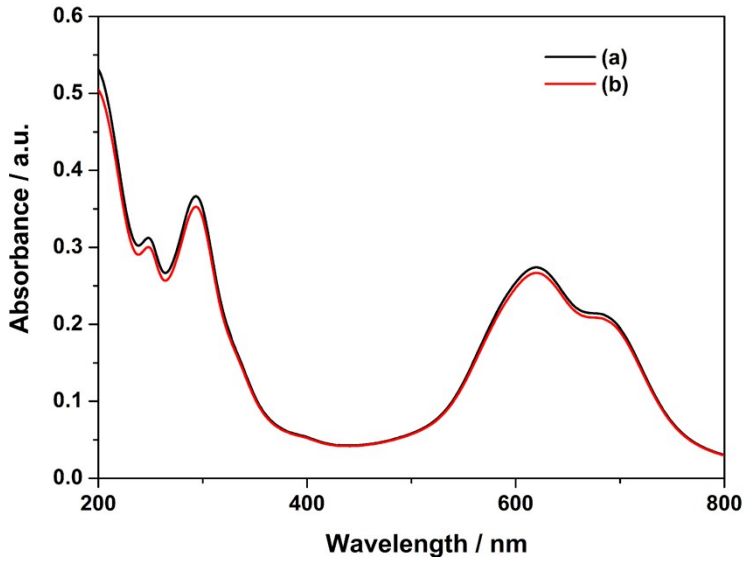

Fig. S24. UV/Vis absorption spectra of (SnR-Co-P_2W_{15}/RhB)$_4$ film on quartz plate before (a) and after (b) dipping in aqueous solution for 2 h